Transitions from Taylor vortex flow in a co-rotating Taylor–Couette system

J. Antonijoan[a)]
Departament Matemàtica i Telemàtica, Universitat Politècnica de Catalunya, Av. Víctor Balaguer s/n, 08800 Vilanova i la Geltrú, Spain

J. Sánchez[b)]
Department Física Aplicada, Universitat Politècnica de Catalunya, c/ Gran Capità s/n, Mod. B5 Campus Nord, 08034 Barcelona, Spain

(Received 12 January 2000; accepted 8 August 2000)

The stability of the Taylor vortex flow in the periodic Taylor–Couette problem with co-rotating cylinders is examined. Transitions to twisted and wavy twisted vortices and wavy inflow and outflow boundary flows are considered. Marginal stability curves for the transition from Taylor to twisted and wavy twisted vortices have been calculated. The azimuthal wave number and the phase velocity at their onset have also been obtained. To compare with experiments and previous numerical works for the narrow gap approximation, the case of radius ratio 0.883 is analyzed in detail. An explanation for the increase in the azimuthal wave number of the twisted vortices as the Reynolds number of the inner cylinder is increased is provided. The velocity fields of twisted vortices, wavy twisted vortices, wavy inflow, and wavy outflow boundary flows at their onset are also shown. © *2000 American Institute of Physics.* [S1070-6631(00)50312-2]

I. INTRODUCTION

Transitions from Taylor vortices in the Taylor–Couette problem have been well studied since the first contributions of some authors at the end of the 1960s. The bifurcations to axisymmetric solutions have been studied in detail [see the review article (Ref. 1)]. Davey *et al.*[2] and Eagles[3] considered nonaxisymmeric perturbations to the basic Couette flow and used weakly nonlinear theories, expanding the solutions in powers of the distance from the inner critical Reynolds number to obtain wavy solutions.

In the early 1980s, Mullin and Benjamin[4] pointed out the strong dependence of the critical Reynolds number for the appearance of wavy vortices with the axial wavelength of Taylor vortices, and Jones[5,6] published his numerical calculations on these transitions showing also the strong dependence with the radius ratio. The discrepancies between the experiments and the theoretical calculations on the selected azimuthal wave number at the onset of the wavy vortex flow, and on the Reynolds numbers at which the bifurcation occurs were explained as end wall effects by Walgraef *et al.*,[7] using amplitude equations, and later by Edwards *et al.*[8] using a Ginzburg–Landau equation. In most of these works, only the case where the outer cylinder is at rest was considered.

After the publication of the works of Andereck *et al.*[9] on new flows on the Taylor–Couette apparatus, the interest in the system with co-rotating cylinders increased. This case was considered in the theoretical studies of Nagata[10,11] and Weisshaar *et al.*[12] They used the narrow gap and almost co-rotating cylinders approximation. With this simplification, the problem becomes mathematically similar to the problem of Rayleigh–Bénard convection of a Boussinesq fluid. In Ref. 12, the transition to twisted vortices was studied; they were calculated and their stability boundaries established. The critical Reynolds numbers were compared with Andereck *et al.* experiments.[9] There was a small shift between experimental data and their calculations, which was attributed to the narrow gap approximation used. It was also shown that the preferred transition was to wavy twisted vortices instead of to twisted vortices for sufficiently high axial wavelength. We show here that similar results are also obtained without the narrow gap approximation, so all these discrepancies must be due to end wall effects, and not to the additional symmetry gained in the narrow gap case.

Transitions to subharmonic solutions from Taylor vortices were first observed by Cole[13] and Lorenzen *et al.*[14] They used the term jet mode to describe these solutions, due to the greater amplitude of the velocity field near the outflow boundaries. In Ref. 9, two subharmonic kinds of bifurcations were reported. The first one corresponds to the jet modes and was named wavy outflow boundaries flow (WOB), because only the outflow boundaries oscillate. The second one was named wavy inflow boundaries flow (WIB) because in this case only the inflow boundaries oscillate. We have obtained the flow patterns of these two kinds of solutions and some results about the transition curves.

The general formulation of the problem is provided in Sec. II, its particular form used for the calculation of Taylor vortices in Sec. II A, their stability in Sec. II B, the numerical methods used in Sec. III, and the results for the stability boundaries and flow patterns are given in Secs. IV A and IV B, respectively.

II. FORMULATION OF THE PROBLEM

We consider the flow of an incompressible fluid confined between two coaxial cylinders, of inner and outer radii r_i^*,

[a)]Electronic mail: fina@fa.upc.es
[b)]Electronic mail: sanchez@fa.upc.es

r_o^* and gap width $d=r_o^*-r_i^*$, which can rotate independently with angular velocities Ω_i, Ω_o. The nondimensional parameters for the problem are the radius ratio $\eta=r_i^*/r_o^*$, and the Reynolds numbers associated with the tangential velocity of the cylinders $R_i=dr_i^*\Omega_i/\nu$, $R_o=dr_o^*\Omega_o/\nu$, where ν is the kinematic viscosity. We use d as length scale and d^2/ν as time scale. The dimensionless Navier–Stokes equations and the incompressibility condition are then

$$\partial_t\mathbf{v}+\mathbf{v}\cdot\nabla\mathbf{v}=-\nabla p+\Delta\mathbf{v},\quad \nabla\cdot\mathbf{v}=0.$$

Using the identity $\mathbf{v}\cdot\nabla\mathbf{v}=\boldsymbol{\omega}\times\mathbf{v}+\nabla(\mathbf{v}^2/2)$, where $\boldsymbol{\omega}=\nabla\times\mathbf{v}$ is the vorticity field, and including $\nabla(\mathbf{v}^2/2)$ into $\tilde{p}$, the Navier–Stokes equations can be written as

$$(\partial_t-\Delta)\mathbf{v}+\boldsymbol{\omega}\times\mathbf{v}=-\nabla\tilde{p},\quad \nabla\cdot\mathbf{v}=0.$$

We will assume infinite cylinders and solutions periodic in the axial direction, of spatial period $\lambda=2\pi/k$. Details on the range of k studied will be given later.

To eliminate the continuity equation and the pressure from the formulation, we use a representation of the velocity field using scalar toroidal and poloidal potentials:

$$\mathbf{v}=\nabla\times(\psi_B\hat{\mathbf{e}}_z)+\nabla\times\nabla\times(\phi_B\hat{\mathbf{e}}_z).$$

This formulation has also been used in the study of the spiral flow.[15] The details of the formulation can be seen in Ref. 16. Here we will only sketch the main lines.

The equations for the potentials ψ_B and ϕ_B are obtained as the z component of the curl and double curl of the original momentum conservation equation:

$$\hat{\mathbf{e}}_z\cdot\nabla\times((\partial_t-\Delta)\mathbf{v}+\boldsymbol{\omega}\times\mathbf{v})=0,$$

$$\hat{\mathbf{e}}_z\cdot\nabla\times\nabla\times((\partial_t-\Delta)\mathbf{v}+\boldsymbol{\omega}\times\mathbf{v})=0.$$

A lengthy but straightforward computation gives

$$(\partial_t-\Delta)\Delta_h\psi_B-\hat{\mathbf{e}}_z\cdot\nabla\times(\boldsymbol{\omega}\times\mathbf{v})=0,$$

$$(\partial_t-\Delta)\Delta\Delta_h\phi_B-\hat{\mathbf{e}}_z\cdot\nabla\times\nabla\times(\boldsymbol{\omega}\times\mathbf{v})=0,$$

with $\Delta_h=D_+D+1/r^2\partial^2_{\theta\theta}$, $D=\partial_r$ and $D_+=D+1/r$. To reduce the order of the equations governing the zero-wave number modes, the following average operators will be used:

$$P_\theta F=\int_0^{2\pi}F(r,\theta,z,t)\,d\theta,$$

$$P_z F=\int_0^{2\pi/k}F(r,\theta,z,t)\,dz.$$

We define f, g, h, ψ, and ϕ as

$$f=-DP_\theta\psi_B,$$

$$g=-DP_\theta\phi_B,$$

$$h=-\Delta_h P_z(1-P_\theta)\phi_B,$$

$$\psi=(1-P_\theta)\psi_B,$$

$$\phi=(1-P_\theta)(1-P_z)\phi_B.$$

The dependence of these potentials is $f=f(t,r,z)$, $g=g(t,r,z)$, $h=h(t,r,\theta)$, $\psi=\psi(t,r,\theta,z)$, and $\phi=\phi(t,r,\theta,z)$ and the following relations hold:

$$P_\theta h=P_\theta\psi=P_\theta\phi=P_z\phi=0. \tag{1}$$

The velocity field can now be written as

$$\mathbf{v}=f\hat{\mathbf{e}}_\theta+h\hat{\mathbf{e}}_z+\nabla\times(g\hat{\mathbf{e}}_\theta+\psi\hat{\mathbf{e}}_z)+\nabla\times\nabla\times(\phi\hat{\mathbf{e}}_z),$$

or, in components

$$\mathbf{v}=\left(-g_z+\frac{\psi_\theta}{r}+\phi_{rz},\ f-\psi_r+\frac{\phi_{\theta z}}{r},h+D_+g-\Delta_h\phi\right). \tag{2}$$

From this latter expression of $\mathbf{v}$ it can be seen that the new potential f is the θ-averaged azimuthal velocity, D_+g is the θ-averaged vertical velocity, and h is the z average of v_z-D_+g.

The equations for these potentials are

$$(\partial_t-\tilde{\Delta})f=-P_\theta\hat{\mathbf{e}}_\theta\cdot\mathbf{u}, \tag{3}$$

$$(\partial_t-\tilde{\Delta})\tilde{\Delta}g=P_\theta\hat{\mathbf{e}}_\theta\cdot\nabla\times\mathbf{u}, \tag{4}$$

$$(\partial_t-\Delta_h)h=-P_z(1-P_\theta)\hat{\mathbf{e}}_z\cdot\mathbf{u}, \tag{5}$$

$$(\partial_t-\Delta)\Delta_h\psi=(1-P_\theta)\hat{\mathbf{e}}_z\cdot\nabla\times\mathbf{u}, \tag{6}$$

$$(\partial_t-\Delta)\Delta\Delta_h\phi=-(1-P_\theta)(1-P_z)\hat{\mathbf{e}}_z\cdot\nabla\times\nabla\times\mathbf{u}, \tag{7}$$

with $\mathbf{u}=\boldsymbol{\omega}\times\mathbf{v}$ and $\tilde{\Delta}=DD_++\partial^2_{zz}$.

The boundary conditions for this system of equations are

$$f(r_i)=R_i,\quad f(r_o)=R_o,$$

and

$$g_z=D_+g=D_+DD_+(P_zg)=0,$$

$$h=0,$$

$$D\psi=\phi=\Delta_h\phi=0,$$

$$\psi_\theta+rD\phi_z=0,$$

$$\Delta\Delta_h\phi_\theta-rD\Delta_h\psi_z=0,$$

on both cylinders. They are obtained from the physical boundary conditions on the cylinders, and from an integral condition needed to make this formulation equivalent to the original Navier–Stokes equations.

A. Equations for the Taylor vortices

The above-mentioned formulation is general for three-dimensional flows and will be used later to find the eigenvalue problem needed to study the stability of Taylor vortices. To calculate these, the formulation can be greatly simplified by using the fact that Taylor vortices are stationary and axisymmetric and that the boundaries that separate two of them are flat. It follows from these last two conditions that

$$h=\psi=\phi=0.$$

The velocity field depends only on r and z, and can be expressed as

$$\mathbf{v}(r,z)=f\hat{\mathbf{e}}_\theta+\nabla\times(g\hat{\mathbf{e}}_\theta)=(-g_z,f,D_+g).$$

This is equivalent to using a streamfunction for the projection of the velocity field onto the $r-z$ plane (g in our case),

plus a function describing the azimuthal velocity (f), as was used in Ref. 5. Now only the first two equations from system (3)–(7) have to be solved. If f and g are separated into their even and odd parts in the periodic direction z, the equations can be also separated, and it is easy to see that f must be even and g must be odd. After expanding the right-hand side of the equations and dropping the dependence on time, the system to be solved to find the Taylor vortices is

$$\tilde{\Delta} f = -g_z D_+ f + f_z D_+ g,$$

$$\tilde{\Delta}\tilde{\Delta} g = \frac{1}{r}\partial_z f^2 + D_+ g \tilde{\Delta} g_z - g_z D_- \tilde{\Delta} g,$$

where $D_- = D - 1/r$, with boundary conditions $f(r_i) = R_i$, $f(r_o) = R_o$, and $g_z = D_+ g = 0$ on both cylinders. We have not written the condition $D_+ D D_+ (P_z g) = 0$ because it is identically satisfied if g is odd.

B. The stability of Taylor vortices

To analyze the stability of Taylor vortices, we will consider only the kinds of perturbations observed in the experiments. So we will restrict our analysis to perturbations with the same axial period $2\pi/k$ as the perturbed vortices, or to subharmonic perturbations with period $4\pi/k$.

If $\mathbf{v}_v(r,z)$ and $\boldsymbol{\omega}_v(r,z)$ are the velocity and vorticity fields corresponding to Taylor vortices, we will consider perturbations of the form

$$\mathbf{v}_p(r,\theta,z,t) = \mathbf{v}_v(r,z) + \mathbf{v}(r,z) e^{\mu t} e^{im\theta}, \tag{8}$$

$m \in Z$ being the azimuthal wave number of the perturbation. In order to obtain subharmonic transitions using perturbations of the same form (8), the basic Taylor vortex flow $\mathbf{v}_v$ with axial periodicity $2\pi/k$ has been extended to an axial period $4\pi/k$. Thus both types of perturbations have been treated in the same way, the only difference being the computational cost.

The perturbations have been written in terms of the scalar potentials for the velocity:

$$f_p(r,z) = f_v(r,z) + f(r,z) e^{\mu t},$$

$$g_p(r,z) = g_v(r,z) + g(r,z) e^{\mu t},$$

$$h_p(r,\theta) = h(r) e^{im\theta} e^{\mu t},$$

$$\psi_p(r,\theta,z) = \psi(r,z) e^{im\theta} e^{\mu t},$$

$$\phi_p(r,\theta,z) = \phi(r,z) e^{im\theta} e^{\mu t}.$$

By substituting these expressions in Eqs. (3)–(7), the following family of eigenvalue problems depending on m is obtained:

$$\mu f = \tilde{\Delta} f - P_\theta \hat{\mathbf{e}}_\theta \cdot \mathbf{u}, \tag{9}$$

$$\mu \tilde{\Delta} g = \tilde{\Delta}\tilde{\Delta} g + P_\theta \hat{\mathbf{e}}_\theta \cdot \nabla \times \mathbf{u}, \tag{10}$$

$$\mu h = \Delta_h h - P_z (1 - P_\theta) \hat{\mathbf{e}}_z \cdot \mathbf{u}, \tag{11}$$

$$\mu \Delta_h \psi = \Delta \Delta_h \psi + (1 - P_\theta) \hat{\mathbf{e}}_z \cdot \nabla \times \mathbf{u}, \tag{12}$$

$$\mu \Delta \Delta_h \phi = \Delta \Delta \Delta_h \phi - (1 - P_\theta)(1 - P_z) \hat{\mathbf{e}}_z \cdot \nabla \times \nabla \times \mathbf{u}, \tag{13}$$

with $\mathbf{u} = \boldsymbol{\omega}_v \times \mathbf{v} + \boldsymbol{\omega} \times \mathbf{v}_v$.

Taylor vortex flow is axisymmetric, and then $P_\theta \mathbf{v}_v = \mathbf{v}_v$ and $(1 - P_\theta)\mathbf{v}_v = 0$. Using this fact, the definitions of f and g, the properties of the operator P_θ acting on the potentials (1) and the linearity of the operator ∇, it is easy to prove the following:

(1) The terms $P_\theta \hat{\mathbf{e}}_\theta \cdot \mathbf{u}$ and $P_\theta \hat{\mathbf{e}}_\theta \cdot \nabla \times \mathbf{u}$, from Eqs. (9) and (10), only depend on the potentials f and g.
(2) The terms $P_z(1 - P_\theta)\hat{\mathbf{e}}_z \cdot \mathbf{u}$ from Eq. (11), $(1 - P_\theta)\hat{\mathbf{e}}_z \cdot \nabla \times \mathbf{u}$ from Eq. (12), and $(1 - P_\theta)(1 - P_z)\hat{\mathbf{e}}_z \cdot \nabla \times \nabla \times \mathbf{u}$ from Eq. (13), only depend on the potentials h, ψ, and ϕ.

Then the eigenvalue problem can be split into two parts. The first two equations (9) and (10) correspond to axisymmetric ($m = 0$) perturbations of Taylor vortices that can be detected while they are being calculated. As we are interested in azimuthal dependence ($m \neq 0$) we will not consider this kind of transition and we will put $f = g = 0$ for the perturbation.

Another splitting of the eigenvalue problem can be obtained by separating the potentials into their even and odd axial components:

$$\psi = \psi^e + \psi^o, \quad \phi = \phi^e + \phi^o.$$

After substituting this potential decomposition in Eqs. (11)–(13), a detailed study of the parity of the terms that appear in each of the equations shows that the system can be separated into two kinds of eigenvalue problems.

Type I:

$$\mu h = \Delta_h h - P_z (1 - P_\theta)(\hat{\mathbf{e}}_z \cdot \mathbf{u})^e, \tag{14}$$

$$\mu \Delta_h \psi^o = \Delta \Delta_h \psi^o + (1 - P_\theta)(\hat{\mathbf{e}}_z \cdot \nabla \times \mathbf{u})^o, \tag{15}$$

$$\mu \Delta \Delta_h \phi^e = \Delta \Delta \Delta_h \phi^e - (1 - P_\theta)(1 - P_z)(\hat{\mathbf{e}}_z \cdot \nabla \times \nabla \times \mathbf{u})^e, \tag{16}$$

and *type II*:

$$\mu \Delta_h \psi^e = \Delta \Delta_h \psi^e + (1 - P_\theta)(\hat{\mathbf{e}}_z \cdot \nabla \times \mathbf{u})^e, \tag{17}$$

$$\mu \Delta \Delta_h \phi^o = \Delta \Delta \Delta_h \phi^o - (1 - P_\theta)(1 - P_z)(\hat{\mathbf{e}}_z \cdot \nabla \times \nabla \times \mathbf{u})^o. \tag{18}$$

In Appendix A, we show the dependence of each right-hand side term of the above equations (14)–(18) on the potentials, once they are separated into their even and odd parts.

The set of boundary conditions for each of the eigenvalue problems are, for case I,

$$h = 0, \tag{19}$$

$$\partial_r \psi^o = \phi^e = \Delta_h \phi^e = 0, \tag{20}$$

$$im\psi^o + r\partial_{rz}\phi^e = 0, \tag{21}$$

$$im\Delta\Delta_h \phi^e - rD\Delta_h \partial_z \psi^o = 0, \tag{22}$$

and for case II

$$\partial_r \psi^e = \phi^o = \Delta_h \phi^o = 0, \tag{23}$$

$$im\psi^e + r\partial_{rz}\phi^o = 0, \tag{24}$$

$$im\Delta\Delta_h \phi^o - rD\Delta_h \partial_z \psi^e = 0, \tag{25}$$

at $r=r_i, r_o$.

The perturbation, $\mathbf{v}$, of the Taylor vortices, $\mathbf{v}_v$, is

$$\mathbf{v}=h\hat{\mathbf{e}}_z+\nabla\times(\psi^o\hat{\mathbf{e}}_z)+\nabla\times\nabla\times(\phi^e\hat{\mathbf{e}}_z)$$

in case I, and

$$\mathbf{v}=\nabla\times(\psi^e\hat{\mathbf{e}}_z)+\nabla\times\nabla\times(\phi^o\hat{\mathbf{e}}_z)$$

in case II. In the latter, the boundaries between vortices are not perturbed and transitions to twisted vortices will be obtained [see the z component of $\mathbf{v}$ in (2)]. In case I, because of the azimuthal oscillations of the boundaries, and following Weisshaar *et al.*,[12] we will name the solutions wavy vortices or wavy twisted vortices, depending on their appearance and azimuthal wave number. Both have oscillatory boundaries, but, as we will show later, the wavy twisted vortices correspond to higher azimuthal wave numbers. When the axial wavelength of the pattern is twice that of Taylor vortices, we will obtain WOB solutions in case I, since all inflow boundaries remain flat while the outflow boundaries of Taylor vortex flow become wavy. In case II, all the outflow boundaries are flat and inflow boundaries become wavy. As a consequence, we will obtain WIB solutions.

III. NUMERICAL METHODS

To examine the stability of the Taylor vortex flow, the first step is to calculate it efficiently. In order to solve the equations for the potentials for the Taylor vortex flow, we have used spectral methods (Canuto *et al.*[17]). The potentials f_v and g_v have been expanded as

$$f_v(x,z)=f_C(x)+\sum_{l=2}^{L}\sum_{n=0}^{N} f_{l,n}H_l^f(x)\cos nkz,$$

$$g_v(x,z)=\sum_{l=4}^{L}\sum_{n=1}^{N} g_{l,n}H_l^g(x)\sin nkz,$$

where f_C is the Couette flow, $f_C=Ar+B/r$, which verifies $f_C(r_i)=R_i$ and $f_C(r_o)=R_o$. The polynomials of degree l H_l^f and H_l^g, are linear combinations of Chebyshev polynomials that verify the boundary conditions $H_l^f=0$ and $H_l^g=D_+H_l^g=0$ on both cylinders. Their expressions can be found in Appendix B. The coordinate $x=2r-(r_i+r_o)$ with $x\in[-1,1]$ has been introduced because of the domain of the Chebyshev functions. The axial wave number k has been included and the axial period is $\lambda=2\pi/k$.

The equations for the amplitudes $f_{l,n}$ and $g_{l,n}$ have been obtained by a collocation method in the two coordinates. We have used a Gauss–Lobatto mesh for the radial coordinate and equally spaced points in the axial direction. This allows an efficient evaluation of the equations for f_v and g_v by using fast trigonometric transforms in both coordinates.

Taylor vortex flows are stationary. Therefore, they can be computed using continuation methods varying different parameters. These techniques are described in detail in Refs. 18–20. They have been previously applied in the Taylor–Couette problem to calculate the bifurcation diagrams for the Taylor vortices (see the reference list in the review article Ref. 1), to compute wavy vortex flows[21] and spiral flows.[15]

Let p be the continuation parameter (R_i, R_o, η, or k), and let X be the vector formed with the amplitudes $f_{l,n}$ and $g_{l,n}$. Then the discretized steady Navier–Stokes equations can be written in the form $F(X,p)=0$. These equations implicitly define a curve of solutions $X=X(p)$ wherever $\det(D_X F(X,p))\neq 0$. At each stage of the continuation process, from the previous known points on the curve of solutions, a predictor step provides the initial guess from which a corrector step, based on a modified Newton–Raphson iteration, converges to a new point on the curve. For the first two steps, the prediction is made using the tangent to the curve; and after, polynomial extrapolation is used based on the last three points on the curve.

The stability of each Taylor vortex solution is obtained during the continuation process. The code that we have developed follows a curve of solutions and stops when a user defined condition $G(X,p)=0$ holds. This procedure has been used with G defined as the real part of the leading eigenvalue of one of the eigenvalue problems already stated (14)–(18).

The eigenvalue problems have also been solved using a collocation method on the same mesh used to obtain Taylor vortices. The expansions for the potentials h, ψ^e, ψ^o, ϕ^e, and ϕ^o are analogous to those for f and g:

$$h(x)=\sum_{l=2}^{L} h_l H_l^h(x),$$

$$\psi^o(x,z)=i\sum_{n=1}^{N}\left[\sum_{l=4}^{L}\psi_{l,n}^o H_{l,n}^{\psi^o}(x)+\sum_{l=6}^{L}\overline{\psi}_{l,n}^o\overline{H}_{l,n}^{\psi^o}(x)\right]\sin nkz,$$

$$\phi^e(x,z)=\sum_{n=1}^{N}\left[\sum_{l=4}^{L}\overline{\phi}_{l,n}^e\overline{H}_{l,n}^{\phi^e}(x)+\sum_{l=6}^{L}\phi_{l,n}^e H_{l,n}^{\phi^e}(x)\right]\cos nkz,$$

$$\psi^e(x,z)=\sum_{n=0}^{N}\left[\sum_{l=4}^{L}\psi_{l,n}^e H_{l,n}^{\psi^e}(x)+\sum_{l=6}^{L}\overline{\psi}_{l,n}^e\overline{H}_{l,n}^{\psi^e}(x)\right]\cos nkz,$$

$$\phi^o(x,z)=i\sum_{n=1}^{N}\left[\sum_{l=4}^{L}\overline{\phi}_{l,n}^o\overline{H}_{l,n}^{\phi^o}(x)+\sum_{l=6}^{L}\phi_{l,n}^o H_{l,n}^{\phi^o}(x)\right]\sin nkz,$$

where $H_l^h, H_{l,n}^{\psi^o}, \overline{H}_{l,n}^{\psi^o}, \overline{H}_{l,n}^{\phi^e}, H_{l,n}^{\phi^e}$, etc., are combinations of Chebyshev polynomials that verify one of the sets of boundary conditions for the potentials (19)–(22) or (23)–(25). In Appendix B the details about the construction of these basis of functions can be found.

To solve the two generalized eigenvalue problems depending on the azimuthal wave number m

$$A_m X=\mu_m B_m X,$$

we have used the LAPACK library. The eigenvectors contain the coefficients $X=(h_l,\psi_{l,n}^o,\overline{\psi}_{l,n}^o,\overline{\phi}_{l,n}^e,\phi_{l,n}^e)$ in case I, and $X=(\psi_{l,n}^e,\overline{\psi}_{l,n}^e,\overline{\phi}_{l,n}^o,\phi_{l,n}^o)$ in case II, and A_m, B_m are complex matrices.

Some tests have been made to ensure that the results are sufficiently accurate. They have been summarized in Tables I and II. With the first we justify why the lower values of m do not appear in any of the subsequent figures. The second shows the degree of accuracy achieved in our calculations for the higher azimuthal wave numbers. In both cases we

TABLE I. Dependence of the inner critical Reynolds number on the truncation parameters L and N for different values of the azimuthal wave number ($m=1,2,12,13$) and of the axial wavelength ($\lambda=1.8,2.1,2.5$) and for $R_o=1060$.

	L	N	$R_{i_c}(\lambda=1.8)$	$R_{i_c}(\lambda=2.1)$	$R_{i_c}(\lambda=2.5)$
	24	12	1275.38	1276.47	1285.53
	24	16	1275.38	1276.46	1286.21
$m=1$	32	12	1365.09	1365.63	1382.86
	32	16	1365.13	1365.66	1369.18
	36	12	1474.65	1476.47	1463.90
	36	16	1475.43	1476.49	1479.07
	48	12	1882.29	1880.17	1837.74
	48	16	1877.07	1873.79	1895.81
	24	12	1289.93	1290.15	1297.84
	24	16	1289.93	1290.12	1299.19
$m=2$	32	12	1400.02	1394.14	1380.36
	32	16	1399.61	1393.34	1393.59
	36	12	1497.48	1500.53	1505.12
	36	16	1497.92	1500.84	1506.81
	48	12	2010.49	1957.45	1890.57
	48	16	1982.74	1972.42	1978.97
	24	12	1364.58	1360.12	1385.81
	24	16	1364.82	1360.12	1383.30
$m=12$	32	12	1491.07	1504.59	1645.98
	32	16	1491.45	1504.04	1644.04
	36	12	1612.64	1689.52	1647.29
	36	16	1594.57	1687.56	1689.82
	48	12	2293.31	2210.43	2064.15
	48	16	2030.41	2209.99	2096.94
	24	12	1369.89	1363.29	1354.58
	24	16	1369.76	1363.44	1356.31
$m=13$	32	12	1487.18	1505.07	1240.43
	32	16	1487.93	1505.48	1240.64
	36	12	1610.92	1661.41	1240.36
	36	16	1598.69	1679.88	1240.63
	48	12	1866.06	1857.17	1240.63
	48	16	1843.15	1828.08	1240.66

TABLE II. Dependence of the critical wavelength λ_c on the truncation parameters L and N for $m=16$ and $m=28$ and for a fixed value of the Reynolds numbers $R_i=1400$ and $R_o=1060$.

	L	N	λ_c
	24	12	1.868
	24	16	1.879
	24	24	1.880
	32	12	2.410
$m=16$	32	16	2.411
	32	24	2.411
	36	12	2.457
	36	16	2.456
	48	12	2.448
	48	16	2.447
	24	12	1.956
	24	16	1.947
	24	24	1.948
	32	12	1.845
$m=28$	32	16	1.845
	32	24	1.845
	36	12	1.821
	36	16	1.820
	48	12	1.823
	48	16	1.824

have solved stability problems of the type II, corresponding to twisted vortices, with $R_o=1060$, the highest outer Reynolds number considered in this study, and for a fixed radius ratio $\eta=0.883$.

In Table I, the values of the inner critical Reynolds number at which Taylor vortices lose stability are shown as a function of the truncation parameters L and N, for azimuthal wave numbers $m=1,2,12,13$ and for three values of the axial wavelength $\lambda=1.8,2.1,2.5$. They have been obtained by increasing the inner Reynolds number R_i because, as can be seen in Table I, the critical inner Reynolds number is not very sensitive to the value of λ for a fixed resolution, in contrast with the results for higher values of m shown in Figs. 1 and 2. In this latter case the curves have been obtained by increasing λ because of the appearance of folds. All the remaining parameters have been kept fixed.

The critical values of R_i, for the azimuthal wave numbers in the range $m=1$ to $m=12$, do not converge with the resolutions we are able to use. They grow as the radial resolution L is increased and seems to be, in general, insensitive to changes in the axial truncation parameter N. They could be even greater than the values we have obtained or the corresponding curves may have folds, as for $m>12$, and they may be at the right of the range of λ considered ($1.6<\lambda<2.5$), as the sequence of curves in Figs. 1 and 2 seems to indicate. Another possibility is that Taylor vortices are stable to some of these kinds of perturbations in the range of values of λ for which they exist.

The case $m=13$ and $\lambda=2.5$ is the only exception in Table I because this curve is the next one to appear at the right in Fig. 2 after $m=14$. The convergence is now quite good showing five stable significant digits.

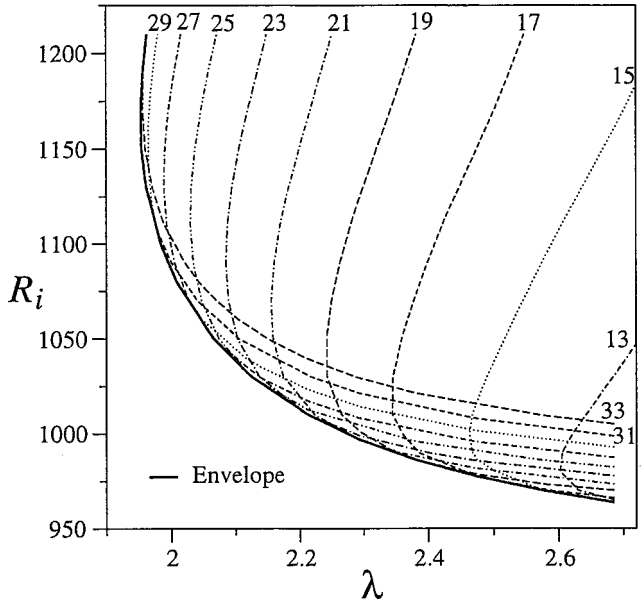

FIG. 1. Marginal stability curves for the onset of twisted vortices of different azimuthal wave numbers. The values of the parameters held constant are $R_o=815$ and $\eta=0.883$.

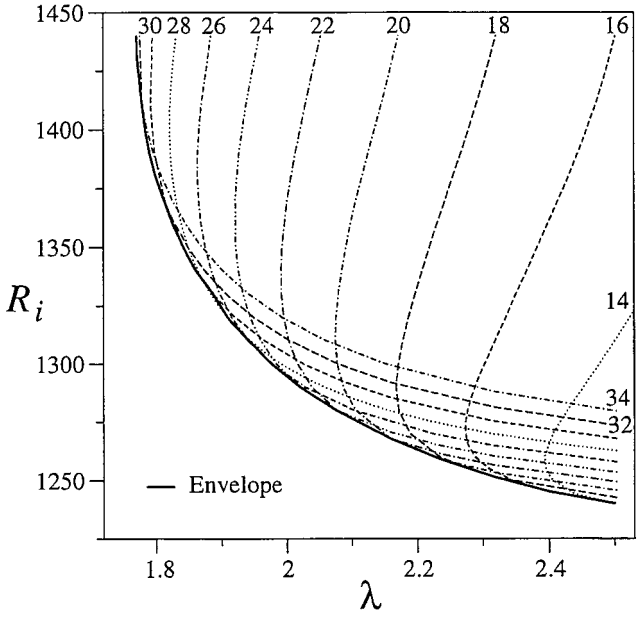

FIG. 2. Marginal stability curves for the onset of twisted vortices of different azimuthal wave numbers. The values of the parameters held constant are $R_o=1060$ and $\eta=0.883$.

In Table II a similar study is shown for azimuthal wave numbers $m=16$ and $m=28$. The Reynolds numbers are $R_i=1400$ and $R_o=1060$ and the critical point has been obtained by increasing λ as explained previously. The value of R_i in the upper region of Fig. 2 has been selected because of the special sensitivity to the truncation parameters. At lower values of R_i the dependence with L and N is not so pronounced.

The results show that the critical point is again much more dependent on L than on N. Doubling N from 12 to 24 (for $L=24$ and $L=32$) only changes, at most, the third significant digit of λ_c. In contrast, to have the same accuracy, at least $L=36$ is needed. The same situation was reported in Ref. 15 for the calculation of the spiral flow.

The resolution used to calculate the curves shown in all the following figures is $L=36$ and $N=12$. Additional checkings of accuracy have been made in some selected points of the curves changing the axial resolution to $N=16$.

IV. RESULTS AND DISCUSSION

A. Stability boundaries

If p and q are two parameters on which Taylor vortices depend (R_i, R_o, η, or k), the neutral curves $\mathrm{Re}(\mu_m)(p,q)=0$ are the boundaries for the onset of tertiary flows with azimuthal wave number m. These curves have been obtained by slicing the parameter plane $p-q$. For a fixed p, the stability of Taylor vortices parametrized by q has been studied to find a point on the neutral curve. This process is repeated for different values of p. In the presence of turning points of $\mathrm{Re}(\mu_m)(p,q)=0$, the role of p and q can be interchanged. We will now present the results for $(p,q)=(\lambda,R_i)$, where $\lambda=2\pi/k$ is the axial wavelength of Taylor vortices.

Although transitions to time-dependent axisymmetric flows are known to exist in the finite length case with the outer cylinder at rest[22] we have focused our attention on nonaxisymmetric bifurcations because we are interested in comparing with experiments performed in co-rotation with a large aspect ratio.

In Figs. 1 and 2 we show the marginal stability curves for the onset of twisted vortices of azimuthal wave number m. For a direct comparison with previous experimental and numerical results, we have taken a fixed gap $\eta=0.883$, and outer Reynolds numbers $R_o=815$ and $R_o=1060$ in Figs. 1 and 2, respectively. Beside each neutral curve we have indicated its corresponding azimuthal wave number, ranging from $m=13$ to $m=34$. As stated before, the curves for $m<13$ are all outside the limits of the plots. Negative values of m correspond to conjugate eigenvalues and eigenfunctions, so only positive values have been considered. We have observed no qualitative difference in the shape of these transition curves by changing the parity of m. Therefore, we have only plotted half of the azimuthal wave numbers in the aforementioned range.

In all the curves the critical R_i number depends strongly on the axial wavelength, and turning points appear. The same behavior has been previously observed in the transition to wavy vortices.[4] The envelope curve of this set of neutral curves has been plotted with solid lines in both Figs. 1 and 2.

The intersections of the neutral curves for numbers m and $m+1$ correspond to bicritical points. At these points, Taylor vortices become unstable and twisted vortices with the same axial wavelength but different azimuthal wave number can appear. Furthermore, complicated dynamics could be observed around these points due to their higher codimension. The nonlinear interaction between these different modes could be the reason why, in the experiments, twisted vortices of different azimuthal wave number can coexist. Bicritical points have also been obtained for the transition to spiral vortices form Couette flow.[23,24]

It is interesting to notice that as the inner Reynolds number is increased with a fixed axial wavelength, transition curves to higher azimuthal wave numbers are crossed. This is consistent with the experiments of Andereck *et al.*[9] They found that, after the onset of the twisted vortices (with wave numbers ranging from 14 to 16 for $\lambda\approx 2.4$), there was a transition in the number of twists to a range of 17 to 20 if the Reynolds number was increased. For other axial wavelengths, they found values of m up to 30. Our results are in good accordance with these experimental results in the values of m and in the order in which they appear.

If only the envelope is considered, as the axial wavelength is increased the first transition occurs at lower inner Reynolds and azimuthal wave numbers. In Ref. 9 it was suggested that this could be the reason why in the experiments the end vortices are the first to bifurcate to twisted ones due to their larger size, when the rest of the Taylor vortices in the core of the fluid are still stable.

In Figs. 3(a) and 3(b), the solid lines are the envelope curves plotted in Figs. 1 and 2, the dashed lines correspond to the calculations of Weisshaar *et al.*,[12] and the triangles to Andereck *et al.*[9] experiments. Our envelopes agree with the

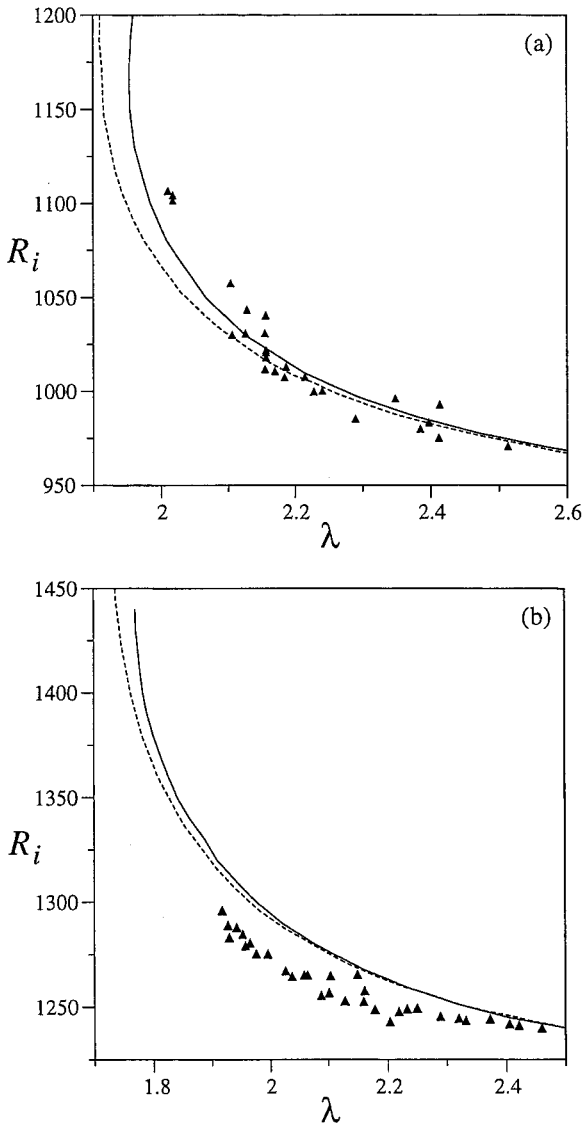

FIG. 3. Comparison of our results with previous ones. The solid lines are the envelopes of the curves of Figs. 1 and 2. The dashed lines correspond to the calculations of Weisshaar *et al.* (Ref. 12), and the triangles are taken from Andereck *et al.* (Ref. 9) experiments. (a) $R_o=815$ and $\eta=0.883$, (b) $R_o=1060$ and $\eta=0.883$.

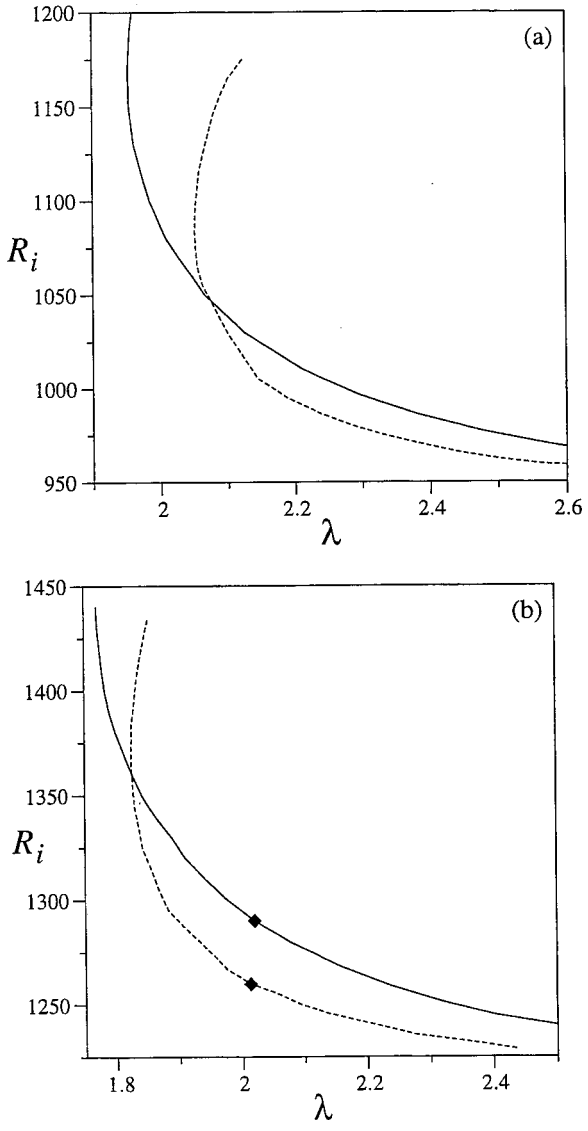

FIG. 4. Boundaries for the onset of twisted (solid line) and wavy twisted vortices (dashed line). (a) $R_o=815$ and $\eta=0.883$. (b) $R_o=1060$ and $\eta=0.883$. The symbols in (b) indicate the position of the eigenfunctions in Figs. 7(b) and 7(c).

stability boundaries obtained in Ref. 12, where narrow gap and almost co-rotating cylinders is assumed, for the higher values of the axial wavelength. There are many possible explanations for the discrepancies for the lower values of λ. They could be due to numerical inaccuracies (although we have shown in Table II that increasing the resolution in our calculations does not change the critical values of λ significantly) or simply to the fact that the two calculations are not for the same value of the radius ratio.

In the case of $R_o=1060$, there is a gap between both numerical results and the experimental ones. Therefore, the assumption of narrow gap and almost co-rotating cylinders is not responsible for this disagreement, which could be due to the effect of the approximation of cylinders of infinite length used in both numerical calculations.

Only twisted vortices seem to have been observed in the experiments of Andereck *et al.*[9] in these regions of parameters. We have also found the neutral curves for the transitions to wavy twisted vortices in order to contrast the numerical results with this experimental evidence. These neutral curves for a fixed *m* are similar to those previously plotted. In Figs. 4(a) and 4(b), the envelopes have been plotted in dashed lines for the same two aforementioned values of R_o. As before, they match, for the higher values of λ, with the transition curves calculated in Ref. 12. The solid lines are the envelopes corresponding to twisted vortices previously shown. The two symbols, one on each curve in Fig. 4(b), indicate the position at which the eigenfunctions have been plotted in Figs. 7(b) and 7(c).

In both our calculations and those of Weisshaar *et al.*[12] the first instability is, above a certain value of λ, to wavy twisted vortices. In Figs. 4(a) and 4(b) this is true for $\lambda>2.07$ if $R_o=815$ and for $\lambda>1.83$ if $R_o=1060$. This behavior differs from the experimental results obtained by Andereck *et al.*[9] In Ref. 12, it is suggested that this is due to the

small gap approximation they used, but as we have shown, both calculations give the same results. We think that this could also be related to the finite length of the cylinders. The effects of the end walls on the two kinds of solutions could be different. The vertical oscillation of wavy twisted vortices would be damped by the end walls, delaying their onset. The twisted vortices would be less affected due to their flat nonoscillatory separation surfaces.

In a recent work,[25] it has been proved that, by periodically forcing the Taylor–Couette system, it is possible to interchange the marginal stability boundaries for the transitions to Taylor vortices and nonaxisymmetric modes. When the outer cylinder is at rest, the first unstable mode is that corresponding to Taylor vortices, but by superposing a vertical periodic oscillation of the inner cylinder it is possible to obtain nonaxisymmetric modes. This has also been reproduced experimentally.[26] It would be interesting to see if by some kind of periodic forcing (vertical oscillations or periodic modulations of the velocity of any of the cylinders) the boundaries for the transitions to twisted and wavy twisted vortices are interchanged. This would provide an experimental way to observe the latter.

We have also made a brief study of the dependence of the onset of twisted vortices with the radius ratio η. Transitions to any other kind of solutions previously mentioned have only been studied for $\eta=0.883$. The results are summarized in Figs. 5 and 6.

Because it is computationally expensive to calculate the envelope curves including all the azimuthal wave numbers, we have only computed the transitions to even values of m. Although this has the consequence that some curves are not smooth, they are informative of the critical Reynolds numbers and of the range of azimuthal wave numbers that could be expected in these cases.

In Fig. 5(a), the even envelopes of the neutral curves corresponding to $\eta=0.7$, 0.75, 0.8, 0.85, 0.883 have been plotted for $R_o=815$. The labels beside each point indicate the corresponding azimuthal wave numbers m.

It can be observed that as η is decreased, the range of m decreases from the range 14–33 for $\eta=0.883$ to 2–6 for $\eta=0.7$. High azimuthal wave number flows are only observed in the case of radius ratios near one. As far as we know, twisted vortices of low m have not been observed in experiments with a wide gap, perhaps because in most cases they have been performed with the outer cylinder at rest, or because the first transition is to wavy vortex flows.

For the smaller radius ratios, the transitions to twisted vortices occurs at a higher inner Reynolds numbers, but if the ratio R_i/R_{i_v} (critical inner Reynolds number for the onset of twisted vortices over inner Reynolds number for the transition to Taylor vortices) is plotted as a function of the axial wavelength λ [Fig. 5(b)], it can be seen that the region of stable Taylor vortices becomes relatively narrower. It is also clear from this figure that for any value of the radius ratio, the Taylor vortices with higher axial wavelength are the first to bifurcate to this kind of solution and that the slope of the curves increases with η.

In Fig. 6, we have compared the phase velocity on the

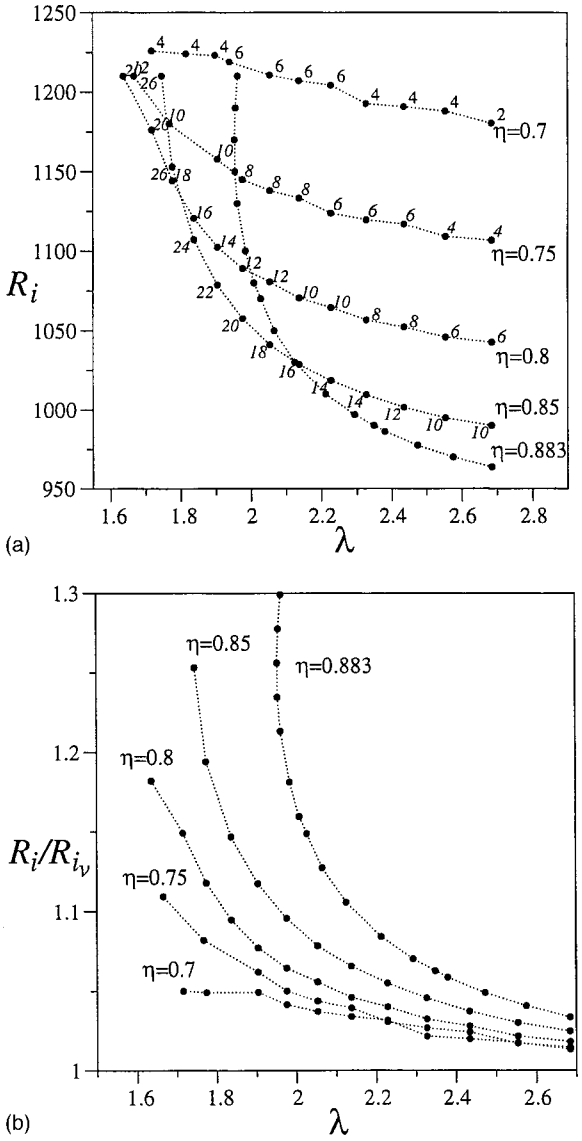

FIG. 5. Boundaries for the onset of even azimuthal wave number twisted vortices for different radius ratios. (a) Inner critical Reynolds number vs λ. (b) Inner critical Reynolds number over inner Reynolds number for the transition to Taylor vortices vs λ. The dominant azimuthal wave numbers are labeled in (a).

even envelopes with the mean angular velocity of the cylinders, both scaled with R_i, for different values of η. From the previous even envelope curves shown in Fig. 5, we have obtained the scaled phase velocity $c=\omega/mR_i$, ω being the imaginary part of the eigenvalue that crosses the imaginary axis at the bifurcation, and R_i the corresponding critical inner Reynolds number. The phase velocity is shown in solid lines and the mean angular velocity with dotted lines. The phase velocity of twisted vortices is almost independent of the axial wavelength. Moreover, as the radius ratio tends to one, this constant is close to the mean angular velocity. An explanation of this behavior was given by Jones[5] for the case of transition to wavy vortices. He suggested that the good agreement he obtained with experiments was due to the fact that the azimuthal velocity of the inviscid core between the cylinders principally determines the phase velocity.

We have not made a detailed study of the subharmonic

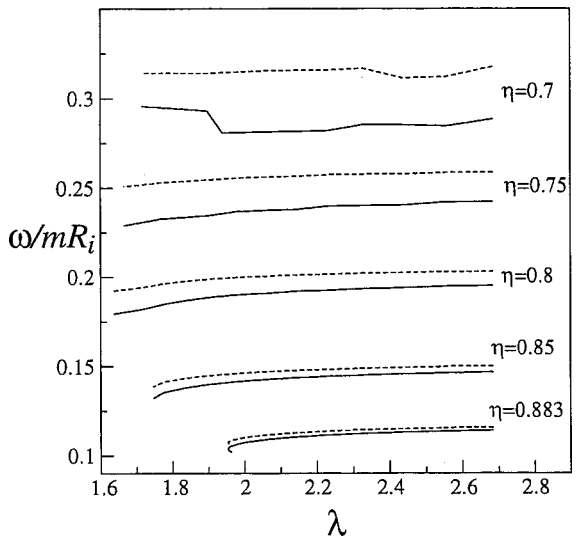

FIG. 6. Relative phase velocities of the twisted vortices at the marginal stability boundaries (solid lines) and mean angular velocity (dotted lines), for different values of η.

transitions because of the high computational cost of solving the eigenvalue problems with twice the vertical resolution of the previous case. Nevertheless, we have computed some critical points to check if they match the experimental results. For WIB flows, the Reynolds numbers at which bifurcations occur are in good agreement with data from Andereck *et al.*,[9] but for WOB flows we have always obtained much lower critical Reynolds numbers. We do not have a good explanation for this fact. It could be due to numerical inaccuracies, which are difficult to check due to the high resolution needed, or to the periodic approximation. In any case, in the following we will show the patterns obtained in both cases. They reproduce the qualitative behavior of these solutions quite well.

B. Flow patterns

In order to obtain a picture of the flow patterns near the bifurcation boundaries, we have added some small multiple of the velocity perturbation field to the axisymmetric velocity field of Taylor vortices. Then the perturbed velocity field is written

$$\mathbf{v}=\mathbf{v}_v+\epsilon(\mathbf{v}_p e^{i\omega t+im\theta}+\overline{\mathbf{v}}_p e^{-i\omega t-im\theta}),$$

where $\mathbf{v}_v$ is the velocity field of Taylor vortices, and $\mathbf{v}_p$ and $\overline{\mathbf{v}}_p$ are the conjugate eigenfunctions with eigenvalues $i\omega$ and $-i\omega$ corresponding to the bifurcations with azimuthal wave number m and $-m$, respectively. In all the plots we have fixed the azimuthal phase by setting $t=0$, i.e.,

$$\mathbf{v}=\mathbf{v}_v+2\epsilon(\mathrm{Re}(\mathbf{v}_p)\cos m\theta-\mathrm{Im}(\mathbf{v}_p)\sin m\theta).$$

The parameters of the flows plotted in all subsequent figures can be seen in Table III.

In Figs. 7(a), 7(b), and 7(c), we show the velocity fields of wavy vortices, twisted vortices, and wavy twisted vortices respectively. The top plot on each group is a perspective view of the projection of each velocity field at radius $r=0.9(r_i-r_o)+r_i$ onto the cylindrical surface of the same radius. In order to obtain a better visualization, we show two vertical periods, and the phase velocity of the whole structure has been subtracted. Then the view would correspond to the rotating frame of reference at which the solutions are stationary. Below each perspective view, we have plotted projections of each velocity field onto five different vertical planes equally spaced in an azimuthal period $2\pi/m$. The left-hand side of each rectangle corresponds to the inner cylinder, and the right-hand side to the outer one. The angular positions of the vertical sections have been indicated in the perspective view.

TABLE III. Value of the parameters for the eigenfunctions shown in this section. In all of them $\eta=0.883$.

Tertiary flows	m	λ	R_o	R_i
Wavy vortices	6	2.00	100.	470.
Twisted vortices	24	2.02	1060.	1290.
Wavy twisted vortices	14	2.01	1060.	1260.
WIB	12	2.00	1100.	1401.
WOB	8	2.00	700.	1051.

The symmetry properties of each of these tertiary flows can be seen in the plots. Twisted vortices keep the reflexion symmetry of Taylor vortices about a horizontal plane because they are solutions of the eigenproblem of type II (17) and (18), so the flat boundaries between them do not suffer any distortion. Wavy and wavy twisted vortices break this symmetry. Both are solutions of the eigenproblem of type I (14)–(16), but the latter have higher azimuthal wave number and are found for higher outer cylinder velocities.

Although the perspective view of twisted and wavy twisted vortices have some similarities, the inclined rope-like structures are quite different. In the first case, the bands with positive and negative slopes are symmetric about the separation plane between vortices and they appear because the perturbation of the Taylor vortex flow moves the center of the vortices from their original position, with a vertical displacement that depends on the azimuthal coordinate. This can be clearly seen in the sequence of vertical plots. In the case of wavy twisted vortices, however, the bands of positive slope are shifted, in the azimuthal direction, from those of negative slope. The bands appear, again, as a consequence of a vertical shift of the vortices. Due to the reflexion symmetry breaking, the two eddies represented in the verticals cuts are not of the same size, as in the case of wavy vortices.

Figures 8(a) and 8(b) show the global structure of subharmonic flows WIB and WOB, respectively. As in previous figures, on top there are perspective views of the velocity fields at radius $r=0.9(r_i-r_o)+r_i$ in Fig. 8(a), and $r=0.2(r_i-r_o)+r_i$ in Fig. 8(b). Different radii have been chosen to make the patterns more evident. The cylinder height is the axial periodicity of the solutions, which is twice that of Taylor vortices. Again, the velocity field at five vertical sections equidistant in an azimuthal period $2\pi/m$ have been plotted below.

The symmetry properties of both subharmonic solutions are clear in the plots. For each of them, one of the two kinds of boundaries between vortices remain flat, the outflow for

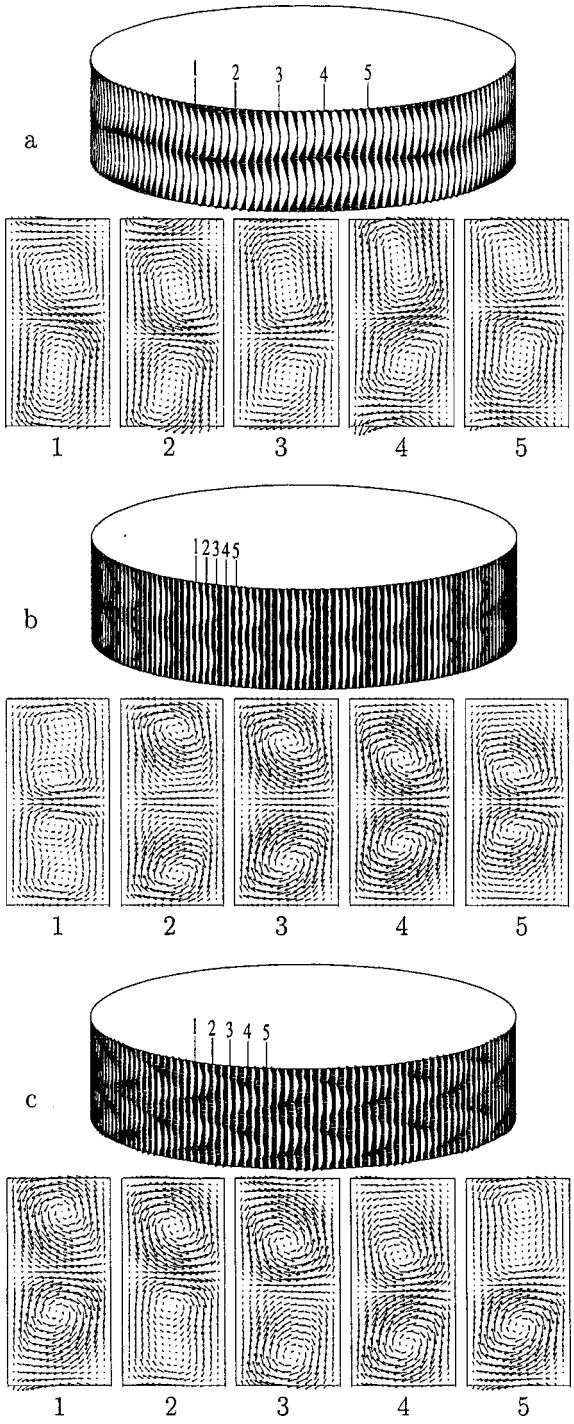

FIG. 7. Velocity fields of (a) wavy vortices, (b) twisted vortices, and (c) wavy twisted vortices of azimuthal wave numbers 6, 24, and 14, respectively. The top plot on each group is a perspective view for radius $r=0.9(r_i-r_o)+r_i$. Below each one are the projections of each velocity field onto five different vertical planes.

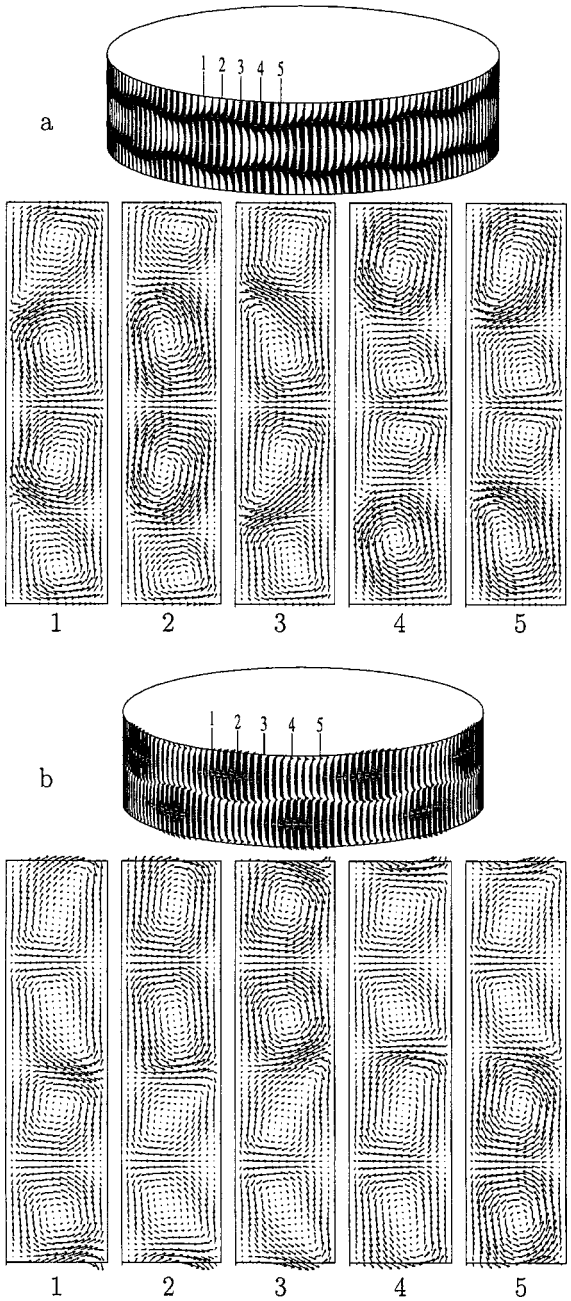

FIG. 8. Velocity fields of (a) WIB and (b) WOB flows of azimuthal wave numbers 12 and 8, respectively. The top plot on each group is a perspective view for radius $r=0.9(r_i-r_o)+r_i$ in (a), and $r=0.2(r_i-r_o)+r_i$ in (b). Below each one are the projections of each velocity field onto five different vertical planes.

WIB and the inflow for WOB, while the other is wavy. The maxima of the velocity are achieved on the wavy boundaries. This was the reason why experimental researchers used the term jet modes. Another well-known characteristic is that the oscillatory boundaries move in antiphase, as can be seen in the perspective views.

V. CONCLUSIONS AND PERSPECTIVES

The transitions from Taylor vortices have been studied. We have compared our results for the transition to twisted vortices with the previous ones from Weisshaar *et al.*,[12] showing that their discrepancies with the experiments of Andereck *et al.*[9] are not due to the narrow gap approximation but to the infinite length approximation. If only the first transition is considered both numerical calculations give very similar results. A possible mechanism for the changes in the azimuthal wave numbers when the inner Reynolds number is increased has been provided. It has also been shown that this

kind of solution with high azimuthal wave numbers is related to narrow gaps. For any value of the radius ratio, the vortices with higher axial wavelength are the first to bifurcate to twisted vortices.

Transition to wavy inflow and outflow boundaries flows have been studied, although in much less detail mainly because of the numerical cost of the computations. For this reason and to start the study of the finite length case (at least for moderate aspect ratios) new numerical methods are needed. We are developing numerical continuation and linear stability analysis techniques based on Arnoldi methods[27] to cope with this and other problems in fluid mechanics.

ACKNOWLEDGMENTS

We thank Marta Net and Francesc Marqués for their helpful comments and suggestions. The European Center for Parallelism of Barcelona (CEPBA) and the Escuela Técnica Superior de Ingenieros de Caminos Canales y Puertos de Barcelona (ETSECCPB) provided most of the computing resources for this research. This work was partially supported by DGESIC Grant No. PB97-0685.

APPENDIX A: DEPENDENCE OF THE EQUATIONS ON THE POTENTIALS

In this Appendix we study the dependence on the potentials h, ψ^o, ψ^e, ϕ^o, ϕ^e of the odd terms $(\hat{\mathbf{e}}_z\cdot\nabla\times\mathbf{u})^o$, $(\hat{\mathbf{e}}_z\cdot\nabla\times\nabla\times\mathbf{u})^o$ and the even terms $(\hat{\mathbf{e}}_z\cdot\nabla\times\mathbf{u})^e$, $(\hat{\mathbf{e}}_z\cdot\nabla\times\nabla\times\mathbf{u})^e$, which are defined as

$$\hat{\mathbf{e}}_z\cdot\nabla\times\mathbf{u}=\frac{1}{r}\mathbf{u}_\theta+\partial_r\mathbf{u}_\theta-\frac{1}{r}\partial_\theta\mathbf{u}_r,$$

$$\hat{\mathbf{e}}_z\cdot\nabla\times\nabla\times\mathbf{u}=\frac{1}{r}\partial_z\mathbf{u}_r-\frac{1}{r}\partial_r\mathbf{u}_z+\partial_{rz}\mathbf{u}_r-\partial_{rr}\mathbf{u}_z-\frac{1}{r^2}\partial^2_{\theta\theta}\mathbf{u}_z+\frac{1}{r}\partial^2_{z\theta}\mathbf{u}_\theta.$$

From these expressions, it is clear that $(\hat{\mathbf{e}}_z\cdot\nabla\times\mathbf{u})^e$, $(\hat{\mathbf{e}}_z\cdot\nabla\times\mathbf{u})^o$, $(\hat{\mathbf{e}}_z\cdot\nabla\times\nabla\times\mathbf{u})^e$, and $(\hat{\mathbf{e}}_z\cdot\nabla\times\nabla\times\mathbf{u})^o$ only depend on the velocities components $\{\mathbf{u}_r^e,\mathbf{u}_\theta^e\}$, $\{\mathbf{u}_r^o,\mathbf{u}_\theta^o\}$, $\{\mathbf{u}_r^o,\mathbf{u}_\theta^o,\mathbf{u}_z^e\}$, and $\{\mathbf{u}_r^e,\mathbf{u}_\theta^e,\mathbf{u}_z^o\}$ respectively.

Let us now split the odd and even part of $\mathbf{u}$ as a function of the potentials, bearing in mind that $\mathbf{u}=\boldsymbol{\omega}_v\times\mathbf{v}+\boldsymbol{\omega}\times\mathbf{v}_v$, where the velocity and vorticity of the Taylor vortices are

$$\mathbf{v}_v=(-g_z^o,f^e,D_+g^o),\quad \boldsymbol{\omega}_v=(-f_z^e,-\tilde{\Delta}g^o,D_+f^e),$$

and the nonaxisymmetric perturbed velocity and vorticity fields are

$$\mathbf{v}=\left(\frac{1}{r}\psi_\theta+\phi_{rz},-\psi_r+\frac{1}{r}\phi_{\theta z},h-\Delta_h\phi\right),$$

$$\boldsymbol{\omega}=\left(\frac{1}{r}h_\theta+\psi_{rz}-\frac{1}{r}\Delta\phi_\theta,-h_r+\frac{1}{r}\psi_{\theta z}+D\Delta\phi,-\Delta_h\psi\right).$$

Then we have

$$\mathbf{u}_r^e=\left(\frac{1}{r}\psi^e_{\theta z}+D\Delta\phi^o\right)D_+g^o+\Delta_h\psi^ef^e-\tilde{\Delta}g^o(-\Delta_h\phi^o)-D_+f^e\left(-\psi_r^e+\frac{1}{r}\phi^o_{\theta z}\right),$$

$$\mathbf{u}_r^o=\left(-h_r+\frac{1}{r}\psi^o_{\theta z}+D\Delta\phi^e\right)D_+g^o+\Delta_h\psi^of^e-\tilde{\Delta}g^o(h-\Delta_h\phi^e)-D_+f^e\left(-\psi_r^o+\frac{1}{r}\phi^e_{\theta z}\right),$$

$$\mathbf{u}_\theta^e=\Delta_h\psi^eg_z^o-\left(\psi^e_{rz}-\frac{1}{r}\Delta\phi^o_\theta\right)D_+g^o+D_+f^e\left(\frac{1}{r}\psi^e_\theta+\phi^o_{rz}\right)+f_z^e(-\Delta_h\phi^o),$$

$$\mathbf{u}_\theta^o=\Delta_h\psi^og_z^o-\left(\frac{1}{r}h_\theta+\psi^o_{rz}-\frac{1}{r}\Delta\phi^e_\theta\right)D_+g^o+D_+f^e\left(\frac{1}{r}\psi^o_\theta+\phi^e_{rz}\right)+f_z^e(h-\Delta_h\phi^e),$$

$$\mathbf{u}_z^e=\left(\frac{1}{r}h_\theta+\psi^o_{rz}-\frac{1}{r}\Delta\phi^e_\theta\right)f^e+\left(-h_r+\frac{1}{r}\psi^o_{\theta z}+D\Delta\phi^e\right)g_z^o-f_z^e\left(-\psi_r^o+\frac{1}{r}\phi^e_{\theta z}\right)+\tilde{\Delta}g^o\left(\frac{1}{r}\psi^o_\theta+\phi^e_{rz}\right),$$

$$\mathbf{u}_z^o=\left(\psi^e_{rz}-\frac{1}{r}\Delta\phi^o_\theta\right)f^e+\left(\frac{1}{r}\psi^e_{\theta z}+D\Delta\phi^o\right)g_z^o+f_z^e\left(\psi_r^e-\frac{1}{r}\phi^o_{\theta z}\right)+\tilde{\Delta}g^o\left(\frac{1}{r}\psi^e_\theta+\phi^o_{rz}\right),$$

where all θ derivatives should be substituted by the product by im.

From these expressions for the velocity components, it can be seen that $\{\mathbf{u}_r^e,\mathbf{u}_\theta^e,\mathbf{u}_z^o\}$ and $\{\mathbf{u}_r^o,\mathbf{u}_\theta^o,\mathbf{u}_z^e\}$ only depend on the set of potentials $\{\psi^e,\phi^o\}$ and $\{h,\psi^o,\phi^e\}$, respectively. Then $(\hat{\mathbf{e}}_z\cdot\nabla\times\mathbf{u})^e$ and $(\hat{\mathbf{e}}_z\cdot\nabla\times\nabla\times\mathbf{u})^o$ only depend on $\{\psi^e,\phi^o\}$, and $(\hat{\mathbf{e}}_z\cdot\nabla\times\mathbf{u})^o$ and $(\hat{\mathbf{e}}_z\cdot\nabla\times\nabla\times\mathbf{u})^e$ only depend on $\{h,\psi^o,\phi^e\}$.

So it has been shown that in the eigenvalue problem of type I only the potentials $\{h,\psi^o,\phi^e\}$ are involved, and that type II only involves $\{\psi^e,\phi^o\}$.

APPENDIX B: CONSTRUCTION OF BASIS FUNCTIONS

In this Appendix we show how to obtain the different basis of functions used to expand the potentials.

The potentials f, h, and g have been expressed in terms of the functions $H_l^f=H_l^h$ and H_l^g, respectively, which verify the boundary conditions $H_l^f=0$ and $H_l^g=D_+H_l^g=0$:

$$H_l^f=\begin{cases}T_l-T_0 & \text{if } l \text{ even}\\ T_l-T_1 & \text{if } l \text{ odd}\end{cases}$$

for $l\geqslant 2$ and

$$H_l^g=\begin{cases}T_l-l^2/4T_2+(l^2/4-1)T_0 & \text{if } l \text{ even}\\ T_l-(1-l^2)/8T_3-(9-l^2)/8T_1 & \text{if } l \text{ odd}\end{cases}$$

for $l \geqslant 4$, T_l being the Chebyshev polynomial of degree l. They can be obtained by the same procedure that is detailed next for the more complicated case of the potentials ψ and ϕ.

The basis for ψ and ϕ cannot be obtained separately due to the coupled boundary conditions. Only the set of boundary conditions corresponding to the type I eigenvalue problem described in Sec. II will be considered in detail. The other type has been treated in a very similar way. Therefore a basis for the pair (ψ^o, ϕ^e) verifying the set of boundary conditions

$$\partial_r \psi^o = \phi^e = \Delta_h \phi^e = 0, \tag{B1}$$

$$im\psi^o + r\partial_{rz}\phi^e = 0, \tag{B2}$$

$$im\Delta\Delta_h \phi^e - rD\Delta_h \partial_z \psi^o = 0 \tag{B3}$$

on both cylinders will be found.

ψ^o and ϕ^e are first expanded in the form

$$\psi^o(x,z) = i\sum_{n=1}^{N} \left(\sum_{l=0}^{L} a_{l,n} T_l(x) \right) \sin nkz,$$

$$\phi^e(x,z) = \sum_{n=1}^{N} \left(\sum_{l=0}^{L} b_{l,n} T_l(x) \right) \cos nkz.$$

If these expressions are substituted into the linear boundary conditions (B1)–(B3), the Fourier coefficients of the resulting equations are relations between the constants $a_{l,n}$ and $b_{l,n}$ that ensure that the boundary conditions will be satisfied. As an example, condition (B2) implies

$$\sum_{l=0}^{L} (ma_{l,n} T_l(x) + rnkb_{l,n} \partial_r T_l(x)) = 0$$

for $n = 1,...,N$ and on the two cylinders ($x = \pm 1$). Boundary conditions are transformed in this way into a set of algebraic relations between the coefficients $a_{l,n}$ and $b_{l,n}$. Therefore we can consider the subset corresponding to a fixed value of n. From these latter ten equations, ten of the coefficients can be expressed in terms of the rest. The dependent coefficients which have been used are

$$\{a_{l,n}\}_{0 \leqslant l \leqslant 3} \quad \{b_{l,n}\}_{0 \leqslant l \leqslant 5}. \tag{B4}$$

These have been chosen because there are two more boundary conditions for ϕ^e than for ψ^o.

Consider now the functions

$$H_{l,n}^{\psi^o}(x) = T_l(x) + \sum_{k=0}^{3} a_{k,n}^l T_k(x),$$

$$\overline{H}_{l,n}^{\phi^e}(x) = \sum_{k=0}^{5} b_{k,n}^l T_k(x), \quad l \geqslant 4,$$

obtained by setting all the independent coefficients to zero except that of T_l in the expansion of ψ^o which is set to one and with $\{a_{k,n}^l\}_{0 \leqslant k \leqslant 3}$ and $\{b_{k,n}^l\}_{0 \leqslant k \leqslant 5}$ satisfying the aforementioned relations between coefficients. The couples $(H_{l,n}^{\psi^o}, \overline{H}_{l,n}^{\phi^e})$ verify (B1)–(B3). Analogously the functions $(\overline{H}_{l,n}^{\psi^o}, H_{l,n}^{\phi^e})$, defined as

$$\overline{H}_{l,n}^{\psi^o}(x) = \sum_{k=0}^{3} a_{k,n}^l T_k(x),$$

$$H_{l,n}^{\phi e}(x) = T_l(x) + \sum_{k=0}^{5} b_{k,n}^l T_k(x), \quad l \geqslant 6,$$

and obtained by setting all the independent coefficients to zero except that of T_l in the expansion of ϕ^e which is set to one, verify the set of boundary conditions.

Finally the expansions used for ψ^o, ϕ^e are

$$\psi^o(x,z) = i\sum_{n=1}^{N} \left[\sum_{l=4}^{L} \psi_{l,n}^o H_{l,n}^{\psi^o}(x) + \sum_{l=6}^{L} \overline{\psi}_{l,n}^o \overline{H}_{l,n}^{\psi^o}(x) \right] \sin nkz,$$

$$\phi^e(x,z) = \sum_{n=1}^{N} \left[\sum_{l=4}^{L} \overline{\phi}_{l,n}^e \overline{H}_{l,n}^{\phi^e}(x) + \sum_{l=6}^{L} \phi_{l,n}^e H_{l,n}^{\phi^e}(x) \right] \cos nkz.$$

[1] S. J. Tavener and K. A. Cliffe, ''Primary flow exchange mechanisms in the Taylor apparatus applying impermeable stress-free boundary conditions,'' IMA J. Appl. Math. **49**, 165 (1991).
[2] A. Davey, R. C. Diprima, and J. T. Stuart, ''On the instability of Taylor vortices,'' J. Fluid Mech. **31**, 17 (1968).
[3] P. M. Eagles, ''On the stability of Taylor vortices by fifth-order amplitude expansions,'' J. Fluid Mech. **49**, 529 (1971).
[4] T. Mullin and T. B. Benjamin, ''Transition to oscillatory motion in the Taylor experiment,'' Nature (London) **288**, 567 (1980).
[5] C. A. Jones, ''Nonlinear Taylor vortices and their stability,'' J. Fluid Mech. **102**, 249 (1981).
[6] C. A. Jones, ''The transition to wavy Taylor vortices,'' J. Fluid Mech. **157**, 135 (1985).
[7] D. Walgraef, P. Borckmans, and G. Dewel, ''Onset of wavy vortex flow in finite geometries,'' Phys. Rev. A **329**, 1514 (1984).
[8] W. S. Edwards, S. R. Beane, and S. Varma, ''Onset of wavy vortices in the finite-length Couette–Taylor problem,'' Phys. Fluids A **3**, 1510 (1991).
[9] C. D. Andereck, R. Dickman, and H. L. Swinney, ''New flows in a circular Couette system with co-rotating cylinders,'' Phys. Fluids **26**, 1395 (1983).
[10] M. Nagata, ''Bifurcations in Couette flow between almost corotating cylinders,'' J. Fluid Mech. **169**, 229 (1986).
[11] M. Nagata, ''On wavy instabilities of the Taylor-vortex flow between corotating cylinders,'' J. Fluid Mech. **88**, 585 (1988).
[12] E. Weisshaar, F. H. Busse, and M. Nagata, ''Twist vortices and their instabilities in the Taylor–Couette system,'' J. Fluid Mech. **226**, 549 (1991).
[13] J. A. Cole, ''The effect of cylinder radius ratio on wavy vortex onset,'' Third Taylor Vortex Flow Working Party Meeting, 1983 (unpublished), p. 1.a1.
[14] A. Lorenzen, G. Pfister, and T. Mullin, ''End effects on the transition to time-dependent motion in the Taylor experiment,'' Phys. Fluids **26**, 10 (1982).
[15] J. Antonijoan, F. Marqués, and J. Sánchez, ''Nonlinear spirals in the Taylor–Couette problem,'' Phys. Fluids **10**, 829 (1998).
[16] F. Marqués, ''On boundary condition for velocity potentials in confined flows: Application to Couette flow,'' Phys. Fluids A **2**, 729 (1990).
[17] C. Canuto, M. Y. Hussaini, A. Quarteroni, and T. A. Zang, *Spectral Methods in Fluid Dynamics* (Springer, New York, 1987).
[18] H. B. Keller, ''Numerical solution of bifurcation and nonlinear eigenvalue problems,'' in *Applications of Bifurcation Theory*, edited by P. H. Rabinowitz (Academic, New York, 1977).
[19] R. Seydel, *Practical Bifurcation and Stability Analysis* (Springer, New York, 1994).
[20] Y. Kuznetsov, *Elements of Applied Bifurcation Theory* (Springer, New York, 1998).
[21] W. Schröder and H. B. Keller, ''Wavy Taylor-vortex flows via multigrid-continuation methods,'' J. Comput. Phys. **91**, 197 (1990).
[22] T. Mullin, K. A. Cliffe, and G. Pfister, ''Unusual time-dependent phenomena in Taylor–Couette flow at moderately low Reynolds numbers,'' Phys. Rev. Lett. **58**, 2212 (1987).
[23] W. F. Langford, R. Tagg, E. J. Kostelich, H. L. Swinney, and M. Golubitsky, ''Primary instabilities and bicriticality in flow between counter-rotating cylinders,'' Phys. Fluids **31**, 776 (1988).

[24]J. Sánchez, ''Simulación numérica en flujos confinados: Estructuras preturbulentas,'' Ph.D. thesis, Universitat de Barcelona, I.S.B.N. 84-475-0945-1, 1994.
[25]F. Marqués and J. M. López, ''Spatial and temporal resonances in a periodically forced hydrodynamic system,'' to be published in Physica D.
[26]A. Y. Weisberg, ''Control of transition in Taylor–Couette flow with axial motion of the inner cylinder,'' Ph.D. thesis, Princeton University, 1996.
[27]W. S. Edwards, L. S. Tuckerman, R. A. Friesner, and D. S. Sorensen, ''Krylov methods for the incompressible Navier–Stokes equations,'' J. Comput. Phys. **110**, 82 (1994).